



Electron paramagnetic resonance study of spin centers related to charge transport in metallic polyaniline

V.I. Krinichnyi^{a,*}, A.L. Konkin^b, A.P. Monkman^c

^a Institute of Problems of Chemical Physics, Russian Academy of Sciences, Academician Semenov Avenue 1, Chernogolovka, 142432 MR, Russia

^b Center for Micro and Nanotechnologies, Technical University of Ilmenau, Gustav-Kirchhoff-Street 7, 98693 Ilmenau, Germany

^c Organic Electroactive Materials Research Group, Department of Physics, University of Durham, South Road, Durham DH1 3LE, United Kingdom

ARTICLE INFO

Article history:

Received 21 January 2012

Received in revised form 18 April 2012

Accepted 24 April 2012

Keywords:

Polyaniline

EPR

Polaron

Dynamics

Relaxation

Conductivity

ABSTRACT

Film-like conducting form of polyaniline (PANI), doped with 10-camphorsulfonic acid (CSA) and 2-acrylamido-2-methyl-1-propanesulphonic acid (AMPSA) has been studied by multifrequency EPR spectroscopy at wide temperature range. Two types of paramagnetic centers with different magnetic resonance and mobility parameters were detected to be stabilized in metal-like domains and amorphous matrix of the samples. Sum spin susceptibility of the samples was shown to consist of the terms originated from paramagnetic centers localized in amorphous polymer backbone as well as spin charge carriers delocalized in embedded metal-like domains. The part of electron spins strongly interacts in the samples that resulting antiferromagnetic term in paramagnetic susceptibility. The delocalized paramagnetic centers characterizing by a stronger Pauli component in spin susceptibility are directly involved in the charge transfer, as compared to the localized ones. Their linewidth is governed by spin precession frequency and dipole–dipole interaction modulated by macromolecular torsional oscillations. The charge was described to be transferred in terms of the Mott quasi-one-dimensional variable range hopping of localized carriers through amorphous bridges between crystalline metal-like domains with mobile carriers interacting with the lattice phonons. The latter process is shown to be accelerated as AMPSA counterion is replaced by CSA one. The activation energy of spin dynamics in crystalline phase inversely correlates with the effective energy separation between localized states. This indicates a major role of dopant structure in local molecular-scale ordering and charge transport properties in doped PANI.

© 2012 Elsevier B.V. All rights reserved.

1. Introduction

Within the class of conducting polymers, polyaniline (PANI) is of special interest for molecular electronics because of its excellent environmental stability combined with high conductivity under ambient conditions [1]. While conductivities as high as 10^5 S/cm have been observed for organic conducting polymers, the bulk conductivity is limited by polymer defects [2], so the transport properties of PANI are well accounted for in terms of “chain-linked mesoscopic granular metal” model [3] proposed for inhomogeneously disordered conducting polymers [4,5]. This model describes PANI as the metallic domains of well-packed and ordered chains in which delocalized electrons produce local conductivity exceeding that of metallic copper. These are embedded in the poorly ordered, amorphous regions, which limit the achievable bulk conductivity to much lower values. Charge transfer in such system is defined by the intradomain hopping and interdomains

tunneling through the amorphous media with strongly localized states. The temperature independent Pauli susceptibility of this system is consistent with the metallic polaron lattice, with a finite density of states $n(\varepsilon_F)$ at the Fermi level (ε_F) [6].

Crystallinity and, therefore, electronic properties of PANI is essentially governed by structure of a dopant introduced. For instance, the Fermi level in PANI doped with sulphuric (PANI-SA) or hydrochloric (PANI-HCA) acid lies in the region of localized states, therefore is considered as a Fermi glass with localized electronic states [7], whereas in PANI highly doped with camphorsulphonic acid (PANI-CSA) the ε_F lies in the region of extended states governing metal behavior of the latter near the metal-insulator boundary [8]. On the other hand, optical (0.06–6 eV) reflectance measurements of e.g. in PANI-CSA [7,9,10] suggest that this polymer is a disordered Drude-like metal near the metal-insulator boundary due to improved homogeneity and reduced degree of structural disorder compared to mineral acid doped PANI. From optical measurements it was determined that the effective charge carrier mass $m^* \approx 2 m_e$, the mean free path $l^* \approx 0.7$ nm and the density of states at the Fermi level $n(\varepsilon_F) \approx 1$ state per eV per two ring repeat units [7,9]. Direct current (dc) conductivity of this polymer has been

* Corresponding author. Tel.: +7 496 522 1882; fax: +7 496 515 5420.

E-mail addresses: kivi@cat.icp.ac.ru, kivirus@gmail.com (V.I. Krinichnyi).

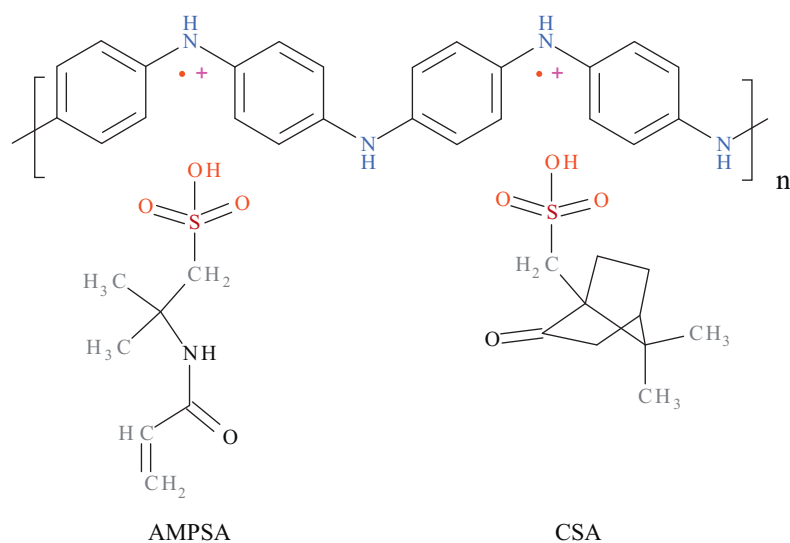


Fig. 1. Chemical structure of polyaniline emeraldine salt and the 2-acrylamido-2-methyl-1-propanesulphonic acid (AMPSA) and camphorsulphonic acid (CSA) used as dopants in the study.

determined to be in the range $\sigma_{dc} \approx 100$ to 350 S/cm at room temperature [11]. Studies of the effect of doping level on both the electronic transport and film morphology of PANI-CSA shown a direct correlation between the degree of crystallinity (induced by hydrogen bonding with the CSA counterion) and its metallic electronic properties [12]. The doping of PANI by another counterion, namely 2-acrylamido-2-methyl-1-propanesulphonic acid (AMPSA) also gives rise to 'metallic' PANI [13]. Hydrogen bonds of these counterions also structure the PANI backbone [14,15], however, in a more complex fashion giving rise to a different crystal structure and lower degree of crystallinity [16]. This allows us to analyze the effect of the microscopic structure on the electronic charge transport in PANI [17]. An opposite signs of magnetoresistance in PANI-CSA and PANI-AMPSA indicates that the ordered mesoscopic regions in PANI-AMPSA are more metallic with respect to that in PANI-CSA [18]. This implies differences in spin relaxation and transport properties, as compared to other doped PANI systems, taking a possibility to develop self-organized metal-like structures in conducting polymers by choosing the appropriate counterions.

Macroscopic *dc* conductivity of the polymers often reflects several electronic processes, so then their intrinsic properties are difficult to be examined because they can be masked by interchain, inter-fibril and other processes. Inhomogeneities in structure and doping can also contribute to this complexity. The electronic processes in PANI-CSA and other organic polymers occur in nanoscales [19]. As in case of other emeraldine salts with doping level y (the number of counterions per polymer unit) lying above the percolation threshold [20,21], intrinsic conductivity and mechanism of charge transfer in the PANI-CSA_{*y*} and PANI-AMPSA_{*y*} systems should also depend on the structure and number of counterion number introduced.

Charge carriers in PANI and other conjugated polymers possess a spin $S = 1/2$, so electron paramagnetic resonance (EPR) method becomes as powerful direct method for the study of different electronic and magnetic properties of such systems, even on the scale of a few polymer units [22,23]. EPR measurement of the paramagnetic susceptibility provides important information on the nature of the electronic states near the Fermi level. EPR study of highly doped PANI-CSA film shown [24,25] that this polymer can be considered as disordered metal near the boundary of the metal-insulator transition which paramagnetic susceptibility is mainly determined by

a temperature independent Pauli contribution at $50 \text{ K} \leq T \leq 300 \text{ K}$, corresponding to $n(\epsilon_F) \approx 1$ state per eV per monomer, and by a temperature dependent Curie contribution below 50 K. This implies that the models that assume transport by spineless bipolarons are not appropriate for PANI-CSA. Lee et al. shown by EPR method [26] that PANI-AMPSA is also inhomogeneous disordered metal near the insulator-metal transition which microwave conductivity (290 S/cm) much greater than that measured by *dc* techniques. Electronic properties of this system are governed by interaction of counterions with polymer backbone [14]. However, despite extensive investigation, there is still not obvious picture concerning electronic and molecular processes in this polymer [27].

Earlier, we have demonstrated that the informativity of the method increases considerably at high spin precession frequencies [21,28]. It was shown [29,30] that two types of paramagnetic centers (PC) with different magnetic, relaxation and dynamics parameters are stabilized in metal-like and amorphous phases of the PANI-CSA and PANI-AMPSA samples.

In this communication we report the results of the study of magnetic and dynamics parameters of highly doped PANI-CSA and PANI-AMPSA samples shown in Fig. 1 at different wavebands EPR. The obtained data confirm the stabilization of two type of PC with different magnetic resonance and dynamics parameters in the polymer regions with different crystallinity. Analysis of the temperature dependencies of paramagnetic susceptibility confirms also the initial thesis that both PANI-CSA and PANI-AMPSA films are disordered metal near the metal-insulator transition with weak electron-electron interaction and that the charge transport properties correlate well with the microscopic structure of the polymer and counterion. The dynamics and mechanism of charge transfer in the polymers are reported as well.

2. Experimental

Film-like high-molecular-weight polyaniline synthesized in Durham at 248 K [31] was used as the started material for PANI-CSA_{*y*} and PANI-AMPSA_{*y*} samples shown in Fig. 1 as films of 20–80 μm thick which were cast from *m*-cresol or dichloroacetic acid solutions onto Si wafers and allowed to dry in air at 313 K. The doping levels $y = [A]/[N]$; A \equiv acid, N \equiv nitrogen site, ranging between 0.4 and 0.6 were achieved by the stoichiometric addition

of acid to polymer. As this process occurs in solution, the doping achieved is both homogeneous and reproducibly stoichiometric.

The direct current (*dc*) conductivities of the films were measured over temperature range of 15–300 K under a dynamic vacuum using standard methodology [30]. The samples were placed in a closed-loop helium cryostat which utilized four platinum contact wires, spaced so that they overlapped four-in-line gold electrodes evaporated on the films. A current of 0.5 mA was passed between the two outer Pt wires and the potential difference measured between the inner two Pt wires. The temperature was changed in steps of 5 K, with conductivity measurements made every 20 min, the current only being applied during each measurement. The samples were found to obey Ohm's law over the current range employed.

The EPR measurements have been performed with a X-band (9.3 GHz, 3-cm) "Thomson", K-band (36.7 GHz, 8-mm) and D-band (140 GHz, 2-mm) EPR spectrometers with a 100-kHz magnetic-field modulation for a phase-lock detection. X-band EPR spectra were recorded in the 14–300 K temperature range with an Oxford ESR cryostat. Total spin concentration in the samples was determined by double integration and comparison of their X-band EPR spectra with that of diphenylpicrylhydrosyl (DPPH) standard. At this waveband, spin susceptibility of mobile centers was determined with an accuracy of 1% and with much greater accuracy for localized centers. The error in the determination of peak-to-peak linewidth ΔB_{pp} and *g*-factor values was ± 0.2 G and $\pm 2 \times 10^{-4}$, respectively. At other wavebands EPR the spectra were obtained at room temperature and dry inert atmosphere.

The simulation of the EPR was performed using OriginPro 7.5 program by application of the methodology outlined below.

3. Results and discussion

3.1. Electron paramagnetic resonance parameters

3.1.1. Calculation of Dysonian line

Normally, X-band EPR spectra of the initial and slightly doped PANI samples exhibit single lines at wide temperature range [20,23]. On the other hand, the increase of the doping level *y* leads to a stabilization in the PANI-CSA and PANI-AMPSA films of two PC with Lorentzian asymmetric lines characterizing by different asymmetry factor *A/B* (the ratio of intensities of the spectral positive peak to negative one) and magnetic resonance parameters (Fig. 2). Such asymmetry of the EPR lines may arise due to unresolved anisotropy of the *g*-factor or the formation of the skin-layer with the thickness δ on the polymer surface as result of interaction of microwave polarizing field with angular frequency ω_e with free charge carriers diffusing inside this skin-layer with *ac* conductivity σ_{ac} . As in the case of other metal-like conjugated polymers [20,23,28,32], this leads to the appearance of the Dyson-like [33] contribution in EPR spectra. The increase in electron precession frequency and polarizing field changes the *A/B* ratio of the samples, however, does not resolve additional components in their EPR spectra (see below). This confirms the assumption that the line asymmetry registered is indeed result from the interaction of microwave field with the charge carriers moving in the conducting polymers under study. The penetration of microwave field into the sample does not exceed δ value, so that the EPR method records only PC inside the skin-layer. This implies that in order to determine more correctly and complete all magnetic resonance parameters of both types PC one should first to calculate their Dysonian spectra as contributions into effective sum spectrum.

If one supposes the slower diffusion of magnetic dipole during T_D than the effective spin-spin (transverse) relaxation time, i.e. $T_D \gg T_2$, in the above compounds [30], both the Dysonian lines

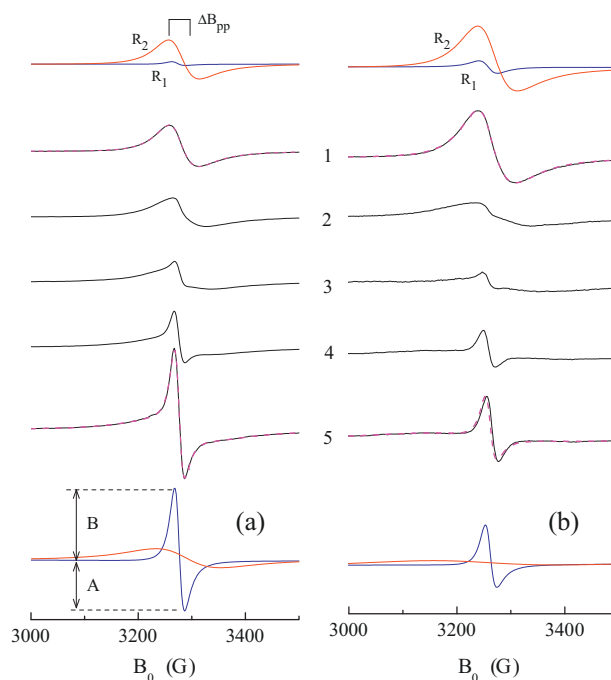


Fig. 2. 3-cm EPR spectra of the PANI-AMPSA_{0.6} (a) and PANI-CSA_{0.6} (b) films registered at 300 K (1), 210 K (2), 130 K (3), 60 K (4), and 30 K (5). The measured parameters *A*, *B*, and ΔB_{pp} are shown. In the top part are shown sum spectra (dashed lines) and their terms *R*₁ and *R*₂ (solid lines) corresponding to deconvolution of a sum of two overlapping Lorentzian lines calculated from Eqs. (1) to (3) using *D:A* = 1:1.8, ΔB_{pp} = 24.2 G (*R*₁) and *D:A* = 18.9:44.6, ΔB_{pp} = 56.3 G (*R*₂) (a) and *D:A* = 0.1:11.3, ΔB_{pp} = 34.3 G (*R*₁) and *D:A* = 55.4:110, ΔB_{pp} = 71.1 G (*R*₂) (b). In the bottom part are shown sum spectra (dashed lines) and their terms *R*₁ and *R*₂ (solid lines) calculated from Eqs. (1) to (3) using *D:A* = 15.2:47, ΔB_{pp} = 18.3 G (*R*₁) and *D:A* = 11.1:49.1, ΔB_{pp} = 120 G (*R*₂) (a) and *D:A* = 15.8:30.9, ΔB_{pp} = 20.6 G (*R*₁) and *D:A* = 40.4:52.9, ΔB_{pp} = 278 G (*R*₂) (b).

should consist of absorption *A_i* and dispersion *D_i* terms, so then the first derivation of absorption spectra can be simulated as

$$\frac{d\chi}{dB} = \sum_{i=1,2} \left[-A_i \frac{2x_i}{(1+x_i^2)^2} + D_i \frac{1-x_i^2}{(1+x_i^2)^2} \right], \quad (1)$$

where $x_i = (B - B_0)/\Delta\omega_L$, B_0 is the resonant magnetic field, $\Delta\omega_L = 1/T_2 \gamma_e$ is Lorentzian line width, and γ_e is the gyromagnetic ratio for electron. In case of the formation of skin-layer on the polymer film with a thickness of $2d$ the coefficients *A_i* and *D_i* in Eq. (1) can be determined from relations [30,34].

$$A_i = \frac{\sinh p + \sin p}{2p(\cosh p + \cos p)} + \frac{1 + \cosh p \cos p}{(\cosh p + \cos p)^2}, \quad (2)$$

$$D_i = \frac{\sinh p - \sin p}{2p(\cosh p + \cos p)} + \frac{\sinh p \sin p}{(\cosh p + \cos p)^2}, \quad (3)$$

where $p = 2d/\delta$, $\delta = \sqrt{2/\mu_0 \omega_e \sigma_{ac}}$, and μ_0 is the magnetic permeability for vacuum. In particular, *ac* conductivity can be determined from the *D_i/A_i*($2d/\delta$) dependence.

Dysonian EPR spectra of the samples calculated from Eqs. (1)–(3) and appropriate magnetic resonance parameters are shown by dashed lines in Fig. 2 as well. The analysis showed that the parameters *A* and *B* of the line asymmetry shown in the figure correlated with the coefficients *A_i* and *D_i* of Eq. (1) as *A/B* = $1 + 1.45D_i/A_i$. The procedure described allowed one to consider each EPR spectra of the PANI-CSA and PANI-AMPSA samples as sum of narrow EPR line of PC *R*₁ radical $\dot{N}-\dot{H}$ with *g* = 2.0028 localized in amorphous polymer matrices and broader EPR spectrum of charge carriers *R*₂ with

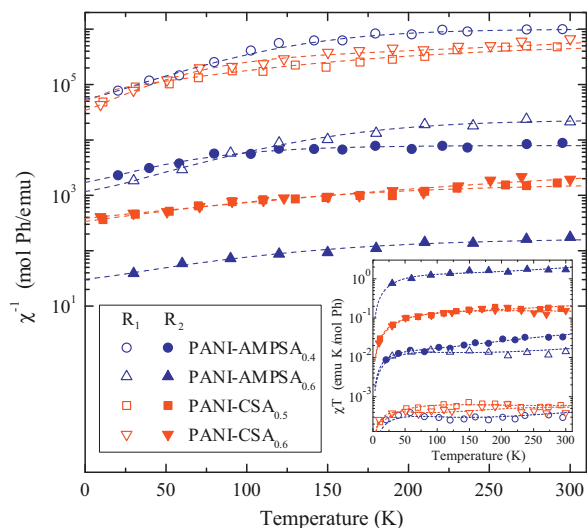


Fig. 3. Temperature dependence of the inversed paramagnetic susceptibility χ^{-1} and χT product (insert) of the PANI-AMPSA $_y$ and PANI-CSA $_y$ samples with different doping levels y . The dashed lines show the dependences calculated from Eq. (4) with respective constants summarized in Table 1.

$g = 2.0020$ diffusing in more ordered, crystalline phase of the polymers. These values were analyzed to be practically independent on the temperature. On the other hand, the shape of EPR spectrum of the PANI samples depends on the temperature, spin precession frequency as well as on the nature and number of counterion. The cooling of the samples leads to the monotonous increase in the linewidth (down to ≈ 25 K) and relative concentration of PC R_2 , as it is seen in Figs. 3 and 4. In the same time, the linewidth of PC R_1 decreases monotonously and their spin concentration increases at the temperature decrease.

3.1.2. Paramagnetic susceptibility

Fig. 3 depicts the effective paramagnetic susceptibility of both the R_1 and R_2 PC with different magnetic resonance parameters as function of temperature. Paramagnetic susceptibility data presented provide important information on the nature of the

electronic states near the Fermi energy level in highly doped, “metallic” PANI samples under study. Sariciftci et al. [24] reported that the Pauli-like contribution predominates in paramagnetic susceptibility of the PANI-CSA film down to 50 K and then it converts into a Curie-like at lower temperatures instead of the conventional Curie plus Pauli behavior typical for other conducting polymers, PANI among them [23,28]. They attributed this effect to the higher ordering of the film with 4–5 meV on-site Coulomb energy and the electron–electron interaction and disorder in the regime of Anderson localization. It is, however, generally difficult to conclude the definite absence of a Curie contribution in the PANI-CSA spin susceptibility, since it is not necessarily a special case for the Pauli susceptibility to depend on the temperature in strongly electron-lattice coupled system [35].

Generally, spin susceptibility of N PC with $S = 1/2$ consists of the Pauli susceptibility of the Fermi gas χ_P as well as a temperature-dependent contributions of localized Curie PC χ_C and the term χ_{ST} coming due to a possible singlet–triplet spin equilibrium in the system [36],

$$\chi = \chi_P + \chi_C + \chi_{ST} = N_A \mu_{\text{eff}}^2 n(\varepsilon_F) + \frac{C}{T} + \frac{k_1}{T} \left[\frac{\exp(-J/k_B T)}{1 + 3 \exp(-J/k_B T)} \right]^2, \quad (4)$$

where N_A is the Avogadro’s number, $\mu_{\text{eff}} = \mu_B g \sqrt{S(S+1)}$ is the effective number of the Bohr magnetons μ_B , $n(\varepsilon_F)$ is the density of states per unit energy (eV) for both spin directions per monomer unit at the Fermi level ε_F , $C = N \mu_{\text{eff}}^2 / 3k_B$ is the Curie constant per mole-C/mole-monomer, k_B is the Boltzmann constant, k_1 is a constant, and J is the antiferromagnetic exchange coupling constant. The contribution of these terms to the total paramagnetic susceptibility depends, e.g. on the nature and mobility of charge carriers.

All the dependences presented in Fig. 3 were fitted by Eq. (4) with the appropriate constants summarized in Table 1. The J values obtained are much lower of the corresponding energy (78 meV) obtained for ammonia-doped PANI [37]. It is seen that at low temperatures when $T \leq T_c \approx 100$ K the Pauli and Curie terms prevail in the total paramagnetic susceptibility χ of both type PC in all PANI samples. At $T \geq T_c$, when the energy of phonons becomes comparable with the value $k_B T_c \approx 9$ meV, the spins start to interact that causes the appearance of the last term of Eq. (4) in sum susceptibility as result of the equilibrium between the spins with triplet and singlet states in the system. It is evident that the R_1 signal susceptibility obeys mainly the Curie law typical for localized isolated PC, whereas the R_2 susceptibility consists of the Curie-like and Pauli-like contributions.

The $n(\varepsilon_F)$ values obtained for the charge carriers in PANI-CSA $_y$ and PANI-AMPSA $_y$ are also summarized in Table 1. This value increases in series PANI-AMPSA $_{0.4} \rightarrow$ PANI-CSA $_{0.5} \rightarrow$ PANI-CSA $_{0.6} \rightarrow$ PANI-AMPSA $_{0.6}$. This density of states of polarons in PANI-CSA is in agreement with that obtained previously in the optical (0.06–6 eV) [7] and EPR [24] studies of this polymer. The Fermi energy of the Pauli-spins was calculated to be $\varepsilon_F \approx 0.2$ eV. This value is lower than the Fermi energy obtained for highly CSA- (0.4 eV) [9] and sulfur- (0.5 eV) [20,38] doped PANI. Assuming again that the charge carrier mass in heavily doped polymer is equal to the mass of free electron ($m_c = m_e$), the number of charge carriers in such a quasi-metal [39], $N_c \approx 4.1 \times 10^{20} \text{ cm}^{-3}$ was determined. This is close to the spin concentration in this polymer; therefore, one can conclude that all delocalized PC are involved in the charge transfer in PANI-CSA $_{0.6}$. The velocity of charge carriers near the Fermi v_F level was calculated to be $3.8 \times 10^7 \text{ cm/s}$ for PANI-CSA that is close to those evaluated for this polymer from the EPR magnetic susceptibility data, $(2.8\text{--}4.0) \times 10^7 \text{ cm/s}$ [40], and $6.2 \times 10^7 \text{ cm/s}$ for PANI-AMPSA.

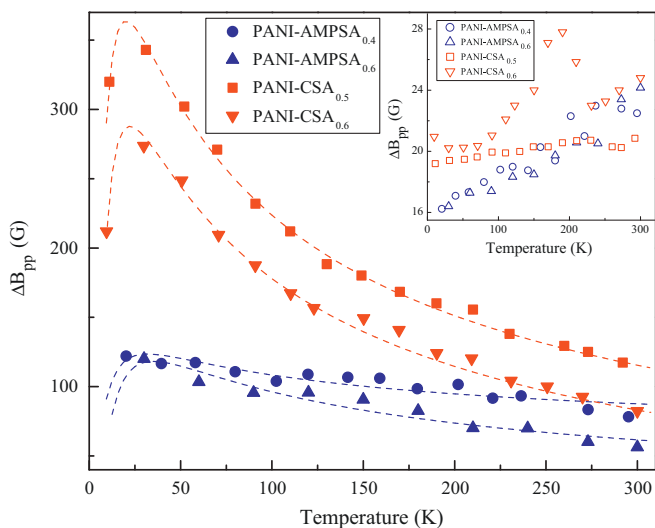


Fig. 4. Temperature dependences of linewidth of the R_1 (insert, open points) and R_2 (filled points) paramagnetic centers stabilized in the PANI-AMPSA $_y$ and PANI-CSA $_y$ samples evaluated using deconvolution of their magnetic resonance spectra. The $\Delta B_{pp}(T)$ dependences calculated from Eq. (7) with respective constants summarized in Table 2 are shown by dashed lines.

Table 1The χ_p , $n(\varepsilon_F)$, C , k_{\parallel} , and J values determined from Eq. (4) for spin charge carriers in different PANI samples at 3-cm waveband EPR.

Polymer	Radical	χ_p , emu/mol one ring	$n(\varepsilon_F)$, states/eV one ring	C , emu K/mol one ring	k_{\parallel} , emu K/mol one ring	J , meV
PANI-AMPSA _{0.4}	R_1	9.8×10^{-7}	–	4.5×10^{-4}	1.5×10^{-2}	0.6
	R_2	1.1×10^{-4}	0.42	7.2×10^{-3}	1.1×10^{-2}	4.8
PANI-AMPSA _{0.6}	R_1	2.2×10^{-5}	–	1.7×10^{-2}	1.7×10^{-2}	4.3
	R_2	5.3×10^{-3}	3.5	6.5×10^{-1}	1.2×10^{-2}	5.9
PANI-CSA _{0.5}	R_1	5.2×10^{-7}	–	2.3×10^{-4}	9.1×10^{-3}	4.5
	R_2	2.7×10^{-4}	1.2	2.7×10^{-2}	1.58	3.6
PANI-CSA _{0.6}	R_1	8.5×10^{-7}	–	4.2×10^{-4}	6.6×10^{-3}	14.3
	R_2	7.1×10^{-5}	1.8	2.2×10^{-2}	2.13	3.8

3.1.3. EPR linewidth

Peak-to-peak linewidth (B_{pp}) of both charge carriers stabilized in the samples is shown in Fig. 4 as function of temperature. It is significant that linewidth of both types of PC is appreciably larger than those obtained previously for the fully oxidized powder-like and film-like PANI-CSA (0.35 and 0.8 G, respectively, at room temperature [24]). The R_1 PC demonstrate linewidth slowly dependent on the temperature that is in good agreement with the rough estimation of the hyperfine interaction between the \dot{N} -H electron and proton distanced by $r \approx 0.1$ nm, $\Delta B_{pp} = \mu_B \mu_p r^{-3} \approx 12$ –15 G (here μ_p is magneton of proton). This value increases as a carrier becomes delocalized, so the magnetic resonance parameters of radicals of the R_2 type clearly reflect the charge transport in the crystalline domains embedded into the PANI-CSA and PANI-AMPSA matrices. This gives also a plausible explanation for the anomalies in the systems under study, which are not observed in other sulfonic acid doped PANI. EPR spectra of the samples may be broadened to some extent by relaxation due to the spin-orbital interaction responsible for linear dependence of T_1^{-1} on temperature [24]; however, this interaction seems to be rather weak in our case. EPR spectrum of PANI could, in principle, be broadened also by the interaction of domestic spins with the oxygen biradicals in PANI doped by hydrochloric acid [41] or/and water vapor in PANI doped by *p*-toluenesulfonic acid [32]. However, in contrast with these samples whom $-NH-$ group is available for air-initiated impurities, such group in the PANI-CSA and PANI-AMPSA backbones is blocked up by counterion forming hydrogen bond with its e.g. $>C=O$ group. This explains the insensitivity of the linewidth of the R_1 and R_2 radicals to the presence of the air [30] and evidences that so broadened lines are intrinsic to the samples under study which electronic properties are indeed defined by hydrogen bonds between $-NH-$ groups and counterions [17]. Such a hydrogen bonding between the $>C=O$ group in both counterions and the $N-H$ group in PANI can lead to closer packing of its chains and, therefore, to better crystallinity. The higher linewidth of both charge carriers in PANI-CSA as compared with PANI-AMPSA (see Fig. 4) could evidences for better molecular scale ordering or crystallinity via the hydrogen bonding in both the phases of the former polymer. This effect can rather indicate a higher conductivity of the PANI-CSA and PANI-AMPSA samples under study. Comparison of the (B_{pp}) values obtained for different PANI-CSA samples suggested that a crystalline phase is formed in their amorphous phase, beginning with the oxidation level $y = 0.3$ [30], and that the PC of this newly formed phase exhibit a broader EPR spectrum.

R_1 radical localized in isolated polymer chain of the polymer amorphous phase is likely indirectly involved in the charge transfer. On the other hand, the linewidth of R_2 paramagnetic centers stabilized in the samples first increases by lowering the temperature from 300 K down to 25 K and then start to decrease at lower temperatures as it was registered earlier also in case of PANI-AMPSA system [14]. This effect evidences for the temperature-assisted delocalization (motional narrowing) of mobile charge carriers like as it was observed for some crystalline ion-radical salts [42]. The temperature dependence of such systems was explained in terms

of the model of molecular torsional oscillations affecting relaxation of whole spin reservoir [43]. According to the model where such oscillations enable intra- and inter-chain spin relaxation to cause broader linewidth, the temperature decrease should stack the oscillations and thereby broadens effective EPR spectrum as

$$\Delta B_{pp} = (\Delta g)^2 (a\tau_{\parallel}^{-1} + b\tau_{\perp}^{-1}), \quad (5)$$

where Δg is the shift of g -factor from g -factor of free electron, $g_e = 2.00232$, a and b are intrinsic constants, τ_{\parallel} and τ_{\perp} are the intra- and inter-chain electron scattering times related as $\tau_{\perp}^{-1} = c|\tau_{\perp}|^2\tau_{\parallel}$, c is a constant, and t_{\perp} is the interchain transfer integral. At the cooling, the intrachain interactions (and τ_{\parallel}) increase strongly, which has a secondary effect on the interchain electron scattering rate τ [43], so then an increase in τ_{\parallel} contributes to the spectrum broadening. Assuming the libration of chains in crystalline metal-like domains in doped PANI [44], the above mentioned phenomenological concept should also be applied to the polymers under study in which the torsional activation motions are expected to be realized with upper frequency of $\nu_t \approx (1-2) \times 10^{13} \text{ s}^{-1}$ [20,21,45]. In this case we can conclude that, in contrast with PANI-AMPSA polymer, the higher linewidth of paramagnetic centers in PANI-CSA system evidences for stronger increase in τ_{\parallel} and, therefore, for higher intrachain conductivity. Dipole-dipole interaction of charge carriers diffusing along and between polymer chains additionally affects EPR linewidth. Such interaction should lead to temperature dependence [46]

$$\Delta B_{pp}(T) = \Delta B_{pp}^{(0)} T^{-1/2} \exp\left(-\frac{E_{dd}}{k_B T}\right), \quad (6)$$

where E_{dd} is the height of the barrier to dipole-dipole interaction. Finally, the EPR linewidth should follows the law

$$\Delta B_{pp}(T) = \Delta B_{pp}^{(0)} T^{-1/2} \exp\left(-\frac{E_{dd}}{k_B T}\right) \exp\left(\frac{E_a}{k_B T}\right), \quad (7)$$

where E_a is the energy for activation of torsional dynamics. The dependences calculated for R_2 charge carriers from Eq. (7) with appropriate E_{dd} and E_a values summarized in Table 2 are also presented in Fig. 4. The figure shows that the temperature dependences of the linewidth determined from the spectra are described well in terms of the above theories. The proximity of the E_{dd} and E_a values should possible evidence the correlation of the molecular libration and spin diffusion processes.

The increase in the polarizing frequency $\nu_e = \omega_e/2\pi$ normally spreads lines of PC in different conducting polymers [21,28], including PANI [20,32,38,47]. However, the room temperature ΔB_{pp} value of charge carriers R_2 in e.g. PANI-AMPSA_{0.6} decreases monotonically with the ν_e increase as it is shown in Fig. 5. This can be in result, e.g., of an acceleration effect of magnetic field growth on spin carriers diffusion [22,23] or/and the decrease in a splitting between individual spin-packets in sum spectra. Indeed, the second order correction to the effective spin-packets resonance field $\delta B = a^2[(I+1) - m^2]/2B_0$ [48] (here $a = 23.7$ G [49] is the constant of hyperfine electron spin coupling with hydrogen nuclei characterizing by spin $I = 1/2$ and orientation magnetic number

Table 2
The $\Delta B_{pp}^{(0)}$, E_{dd} , and E_a values obtained for charge carriers R_2 stabilized in different doped PANI samples from the fitting of their $\Delta B_{pp}(T)$ experimental data by Eq. (7) as well as $T_{2(0)}$, $\tau_c^{(0)}$, and E_b values determined from the fitting of their $T_2(T)$ dependences by Eq. (9).

Polymer	$\Delta B_{pp}^{(0)}$, G	E_{dd} , meV	E_a , meV	$T_{2(0)}$, s	$\tau_c^{(0)}$, s	E_b , meV
PANI-AMPSA _{0.4}	681	15	13	5.8×10^{-10}	7.4×10^{-8}	50
PANI-AMPSA _{0.6}	1176	15	14	6.4×10^{-10}	6.3×10^{-8}	43
PANI-CSA _{0.5}	3130	31	30	2.1×10^{-10}	3.4×10^{-7}	13
PANI-CSA _{0.6}	2802	31	30	2.0×10^{-10}	3.7×10^{-7}	7.2

$m = \pm 1/2$) should decrease from 44 mG down to 2.8 mG at the ν_e increases from 9.3 up to 140 GHz. Besides, the probability P_{Cr} of cross-relaxation of the spin-packets in real solids depends on ν_e as [50]

$$P_{Cr} = 2\pi \sqrt{\langle \omega^2 \rangle} \exp\left(-\frac{\nu_e^2}{2\langle \omega^2 \rangle}\right), \quad (8)$$

where $\langle \omega^2 \rangle = 9/20 \gamma_e^2 \hbar^2 d^{-6}$ is the lattice sum for powder-like sample, d is a distance between spins, and $\hbar = h/2\pi$ is the Plank constant. If one assume that the linewidth of paramagnetic centers in the PANI sample changes as $\Delta B_{pp}(\nu_e) = 5.33 + 53.2 \exp(-9.27 \times 10^{-22} \nu_e^2)$ G, so then the lower limit for linewidth at $\nu_e \rightarrow 0$ and $d \approx 6.9$ nm can be determined to be 5.33 G.

3.2. Spin relaxation and dynamics

The relaxation processes in magnetic systems normally occur by interaction of half-integer electron and/or nuclear spins with additional magnetic fields, produced by magnetic dipoles of other nucleus and electrons, which are fluctuating due to their random rotational and translational walk. The spin-spin (transverse) electron spin relaxation rate for a dipole-dipole interaction between the mobile electron spins can be expressed by the relation [51]

$$T_{2(0)}^{-1}(\omega_0) = T_{2(0)}^{-1} + \langle \omega_D^2 \rangle [0.3J(0) + 0.5J(\omega_0) + 0.2J(2\omega_0)], \quad (9)$$

where $T_{2(0)}$ is spin-spin relaxation provoked by localized spin interactions with, e.g., protons, $\omega_D = \gamma_e^2 \hbar \sqrt{nS(S+1)} \sum r_{ij}^{-3}$ is the dipolar coupling constant for powder (in rad/s), n is the number of spins per monomer unit, $\sum r_{ij}$ is lattice sum, r_{ij} is a spin separation, and $J(\omega)$ is a spectral density induced by modulation of dipole and hyperfine coupling due to the diffusion of the electron spins. The dynamics of spin carriers in metal-like domains

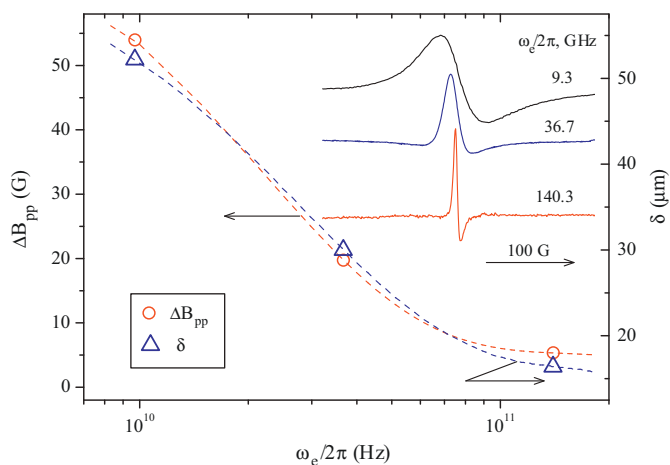


Fig. 5. Room-temperature EPR spectra of the PANI-AMPSA_{0.6} sample obtained at different electron spin precession frequency $\omega_e/2\pi$ and the dependence of absorption linewidth the R_2 paramagnetic centers (ΔB_{pp}) and the depth of skin-layer (δ) initiated by these charge carriers in this sample as function of the ω_e . The lines are drawn to guide the eye.

embedded into polymer amorphous phase can rather be described in terms of their 3D diffusion over a barrier E_b per correlation time $\tau_c = \tau_c^{(0)} \exp(E_b/k_B T)$ originating a spectral density function $J(\omega_e) = \tau_c / (1 + \tau_c^2 \omega_e^2)$ [51]. In this case, the τ_c value is essentially the average time required for a spin charge carrier to move through a distance equal to its delocalization length.

As can be seen from Fig. 6, the $T_2(T)$ dependencies obtained experimentally for PANI-CSA_y and PANI-AMPSA_y systems are well described by Eq. (9) with appropriate parameters summarized in Table 2. The higher E_b values obtained for both the PANI-AMPSA_y samples as compared to the PANI-CSA_y ones can be assigned to the better ordering of metal-like domains in the latter system.

3.3. DC and AC conductivity

The number and dynamics of each type of charge carriers differ, thus the electronic properties of the samples should depend on both the structure and number of counterions. In order to determine this correctly the analysis of both the *dc* and *ac* conductivities was made. These parameters determined for the PANI-CSA_y and PANI-AMPSA_y films with $y \geq 0.4$ from their *dc* conductometry [30] and Dysonian spectra are given in Fig. 7 as function of temperature. The room temperature σ_{dc} determined for highly doped PANI-CSA lies near that (100–350 S/cm) earlier obtained for this sample [11]. The analysis shown, that these dependences are governed by parallel diffusion of charge carriers through amorphous and crystalline regions of polymer and, therefore, can be described in framework of two models. One of them is the Mott Q1D variable range hopping (VRH) model [52] of localized charge carriers between crystalline high-conducting regions through amorphous bridges (the semi-conducting regime). This should result in temperature dependence

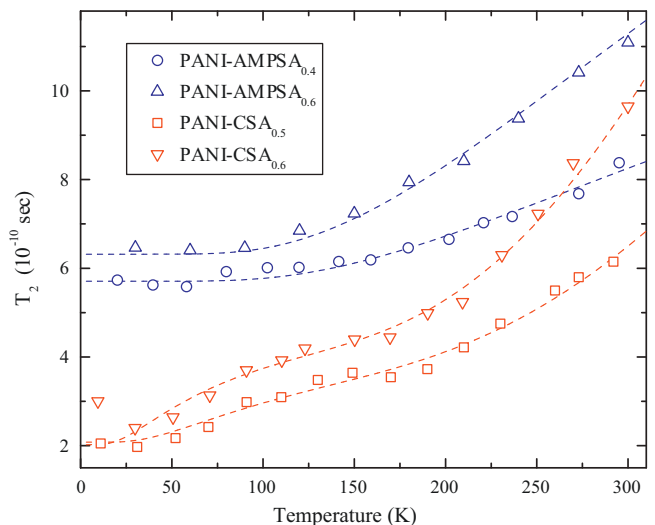


Fig. 6. Temperature dependences of spin-spin relaxation of the R_1 and R_2 centers stabilized in the PANI-AMPSA_y and PANI-CSA_y samples. The dotted lines show dependences calculated from Eq. (9) with respective constants summarized in Table 2.

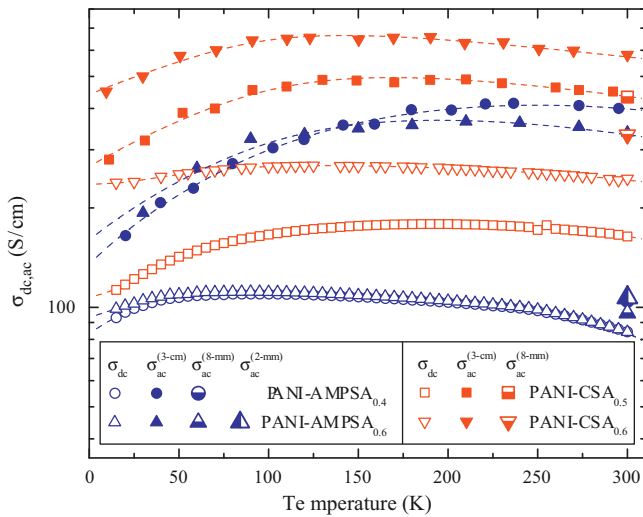


Fig. 7. Temperature dependence of *dc* (open symbols) conductivity measured conductometrically and *ac* (filled symbols) conductivity determined from 3-cm, 8-mm, and 2-mm wavebands EPR Dysonian spectra of the R_2 paramagnetic centers stabilized in the PANI-AMPSA_y and PANI-CSA_y samples. Dashed lines show the dependences calculated from Eqs. (13) and (14) with respective constants summarized in Table 3.

of both the *dc* and *ac* conductivities of such a system as [53]

$$\begin{aligned} \sigma_{dc}(T) &= 0.39\omega_0 e^2 \left[\frac{n(\varepsilon_F)(L)}{k_B T} \right]^{1/2} \exp \left[-\left(\frac{T_0}{T} \right)^{1/2} \right] \\ &= \sigma_{dc}^{(0)} T^{-1/2} \exp \left[-\left(\frac{T_0}{T} \right)^{1/2} \right], \end{aligned} \quad (10)$$

$$\sigma_{ac}(T) = \frac{1}{3} \pi e^2 k_B T n^2(\varepsilon_F) \langle L \rangle^5 \omega_e \left[\ln \frac{\omega_0}{\omega_e} \right]^4 = \sigma_{ac}^{(0)} T, \quad (11)$$

where ω_0 is a hopping attempt frequency, e is an elemental charge, $\langle L \rangle$ is the average length of charge wave localization function, $T_0 = 16/k_B n(\varepsilon_F) z \langle L \rangle$ is the percolation constant or effective energy separation between localized states depending on disorder degree in amorphous regions, z is the number of nearest-neighbor chains. It should be noted, that the 3D VRH model gives abnormal low T_0 value for all the samples studied.

Diffusion of charge carriers in more crystalline, metal-like clusters embedded into polymer matrices can obviously be governed by their scattering on the lattice optical phonons which should result the following temperature dependence of the PANI intrinsic conductivity [2,54]

$$\begin{aligned} \sigma(T) &= \frac{Ne^2 c_{1D}^2 M t_0^2 k_B T}{8\pi \hbar^3 \alpha_{eph}^2} \left[\sinh \left(\frac{E_{ph}}{k_B T} \right) - 1 \right] \\ &= \sigma_0 T \left[\sinh \left(\frac{E_{ph}}{k_B T} \right) - 1 \right], \end{aligned} \quad (12)$$

where c_{1D} is the lattice constant, M is the mass of the polymer unit, t_0 is the transfer integral, E_{ph} is the energy of the optical phonons, and α_{eph} is the constant of electron–phonon interaction.

Both the $\sigma_{dc}(T)$ and $\sigma_{ac}(T)$ dependences presented in Fig. 7 demonstrate non-monotonous plateaus shape. Note, that the analogous $\sigma_{ac}(T)$ dependence was obtained for highly doped PANI-CSA_y sample at 6.5 GHz by using *ac*-conductometry method [55]. This can be attributed to the above-mentioned interaction of charge carriers with lattice phonons at high temperatures in parallel with their Mott VRH at low temperatures. In this case the charge transfer should consist of two successive processes, so then the *dc* and *ac* conductivities should be expressed as a combination of Eqs. (10) and (12) as well as Eqs. (11) and (12), respectively:

$$\begin{aligned} \sigma_{dc}^{-1}(T) &= \sigma_{dc(0)}^{-1} + \sigma_1^{-1} T^{1/2} \exp \left[\left(\frac{T_0}{T} \right)^{1/2} \right] \\ &+ \sigma_2^{-1} T^{-1} \left[\sinh \left(\frac{E_{ph}}{k_B T} \right) - 1 \right]^{-1}, \end{aligned} \quad (13)$$

$$\sigma_{ac}^{-1}(T) = \sigma_{ac(0)}^{-1} + \sigma_3^{-1} T^{-1} + \sigma_4^{-1} T^{-1} \left[\sinh \left(\frac{E_{ph}}{k_B T} \right) - 1 \right]^{-1} \quad (14)$$

Fig. 7 shows that *dc* conductivity of the polymers experimentally obtained is fitted well by Eq. (13) with parameters summarized in Table 3. In contrast with other conducting polymers, lower T_0 parameter is characteristic for these samples. This is evidence of the longer averaged length of charge wave localization function in the samples. Indeed, $\langle L \rangle$ value was determined for PANI-CSA_{0.6}, PANI-CSA_{0.5}, PANI-AMPSA_{0.4}, and PANI-AMPSA_{0.6}, to be 17, 37, 264, and 239 nm, respectively.

AC conductivity of the polymers is also reflects the above mentioned successive parallel mechanisms, so the experimental data can be circumscribed by Eq. (14). Indeed, it is seen from Fig. 7 that the $\sigma_{ac}(T)$ dependences obtained experimentally for R_2 PC in all systems studied are fitted well by Eq. (14) with appropriate parameters summarized in Table 3. The energy determined for phonons in these PANI samples lies near to that obtained for other polymers [20,28] and evaluated (66 meV) from the data determined by Wang et al. for hydrochloric-acid-doped PANI [5].

Thus, main PC are localized in the highly doped PANI-CSA and PANI-AMPSA samples at low temperatures. This originates the Curie type of susceptibility of the samples and the VRH charge transfer between their polymer chains. The spin–spin exchange is stimulated at high temperature region due likely to the activation librations of the polymer chains [44].

The E_{ph} and $\langle L \rangle$ values determined above for mediatory doped samples correlate. This means that the higher the $\langle L \rangle$ value, the stronger interaction of PC with phonons in metal-like crystallites. There is some tendency in the increase of $RT \sigma_{dc}$ and σ_{ac} conductivities in the series PANI-AMPSA_{0.6} → PANI-AMPSA_{0.4} → PANI-CSA_{0.5} → PANI-CSA_{0.6} “feeling” by the R_2 PC. The data obtained can be evidence of indirect contribution of the R_1

Table 3

The $\sigma_{dc(0)}$, σ_1 , T_0 , σ_2 , E_{ph} values determined from the fitting of σ_{dc} by Eq. (13), and $\sigma_{ac(0)}$, σ_3 , σ_4 , and E_{ph}^l ones determined from the fitting of σ_{ac} by Eq. (14) for different doped PANI samples.

Polymer	$\sigma_{dc(0)}$, S/cm	σ_1 , K ^{1/2} S/cm	T_0 , K	σ_2 , S/cmK	E_{ph} , meV	$\sigma_{ac(0)}$, S/cm	σ_3 , S/cm K	σ_4 , S/cm K	E_{ph}^l , meV
PANI-AMPSA _{0.4}	86.4	1152	209	0.308	22	135	1.68	1.57	37
PANI-AMPSA _{0.6}	95.2	1094	277	0.181	20	160	1.62	0.76	39
PANI-CSA _{0.5}	109.6	5757	521	1.65	28	267	1.99	0.68	39
PANI-CSA _{0.6}	236.6	5462	753	0.286	24	441	2.27	0.64	36

PC and direct contribution of the R_2 PC in the charge transfer through respectively amorphous and crystalline parts of the polymers. RT σ_{ac} values determined from Dysonian spectra of R_2 PC lies near respective σ_{dc} values that is characteristic for classic metals.

Therefore, charge transport between crystalline metal-like domains occurs through the disordered amorphous regions where the charge/spin carriers are more localized as it was predicted for a disordered metal close to the critical regime of the metal-insulator transition with the Fermi energy close to the mobility edge [24,25]. The assumption that higher purity PANI coupled with homogeneous doping would give rise to no EPR signal, characteristic of a purely bipolaronic matrix, is in contradiction with the increase of ac conductivity with spin concentration in polymer systems. Both PANI-CSA and PANI-AMPSA reveal better electronic properties over PANI with other dopants, as shown by their electrical conductivity which is both greater in magnitude and follows metallic temperature dependence.

4. Conclusions

So, two types of PC are formed in PANI, polarons localized on chains in amorphous polymer regions and polarons diffusing in crystalline domains of strongly coupled polymer chains. The latter factor plays an important role in the stabilizing of the metallic state, when both Q1D electron localization and “Peierls instability” are avoided. Above the percolation threshold the interaction between spin charge carriers becomes stronger, so part of the mobile polarons collapses into diamagnetic bipolarons. Besides, the doping changes the interaction of the charge carriers with the lattice phonons, and therefore the mechanism of charge transfer. It also results in an increase of the number and size of ordered crystalline domains with delocalized charge carriers, which lead to an increase in the conductivity and Pauli term in sum paramagnetic susceptibility. These carriers are directly involved in the charge transfer; their dynamics is governed by the lattice phonons and molecular torsional oscillations. This mechanism is accompanied by parallel indirect Mott Q1D variable range hopping of localized charge carriers between crystalline domains through amorphous bridges. A strong Pauli susceptibility of the spin species associated with the broad EPR lines indicates intrinsically metallic character of Q3D crystalline domains in PANI-AMPSA and PANI-CSA samples. The energy required for activation of spin dynamics across crystalline phase inversely correlates with the effective energy separation between localized states. The charge transfer is accelerated at the replacement of AMPSA counterion by CSA one. This evidences a major role of dopant structure in local molecular-scale ordering and charge transport properties in doped PANI. Our results confirm the heterogeneous structure for PANI-CSA and PANI-AMPSA films, typically crystalline highly conducting domains embedded into amorphous less conducting regions which control the ac and dc conductivities, respectively. In conclusion our study of several highly doped PANI conducting films shows that electronic processes concern some scales. At the chain scale, microwave (EPR) conductivity let intrinsic PANI metallic behavior appear, whereas static conductivities reveal the importance of long-range correlations and cluster effects.

Acknowledgments

This study was supported in part by the Royal Society (Grant No. 638072.P885/bll) and the Russian Foundation for Basic Researches (Grant No. 12-03-00148).

References

- [1] A.J. Heeger, *Journal of Physical Chemistry B* 105 (2001) 8475–8491; M. Fahlman, X. Crispin, J.A.O. Smallfield, R. Lazzaroni, J.L. Bredas, S. Li, Y. Wei, A.J. Epstein, *Electroactive Polymers for Corrosion Control*, 2003, pp. 76–89; B. Wessling, in: T.A. Skotheim, J. Reynolds (Eds.), *Conjugated Polymers: Processing and Applications*, 3rd ed., CRC Press, Boca Raton, 2006, pp. 3–75; S. Bhadra, *Polyaniline: Preparation, Properties, Processing and Applications*, Lap Lambert Acad. Publ., 2010.
- [2] S. Kivelson, A.J. Heeger, *Synthetic Metals* 22 (1988) 371–384.
- [3] V.N. Prigodin, A.J. Epstein, *Europhysics Letters* 60 (2002) 750–756.
- [4] Z.H. Wang, A. Ray, A.G. MacDiarmid, A.J. Epstein, *Physical Review B* 43 (1991) 4373–4384; R.S. Kohlman, A.J. Epstein, in: T.A. Skotheim, R.L. Elsenbaumer, J.R. Reynolds (Eds.), *Handbook of Conducting Polymers*, Marcel Dekker, Inc., New York, 1997, pp. 85–122.
- [5] Z.H. Wang, C. Li, E.M. Scherr, A.G. MacDiarmid, A.J. Epstein, *Physical Review Letters* 66 (1991) 1745–1748; Z.H. Wang, E.M. Scherr, A.G. MacDiarmid, A.J. Epstein, *Physical Review B* 45 (1992) 4190–4202.
- [6] C. Fite, Y. Cao, A.J. Heeger, *Solid State Communications* 70 (1989) 245–247.
- [7] K. Lee, A.J. Heeger, Y. Cao, *Synthetic Metals* 72 (1995) 25–34.
- [8] M. Reghu, Y. Cao, D. Moses, A.J. Heeger, *Physical Review B* 47 (1993) 1758–1764; C.O. Yoon, M. Reghu, D. Moses, A.J. Heeger, Y. Cao, *Physical Review B* 48 (1993) 14080–14084.
- [9] K.H. Lee, A.J. Heeger, Y. Cao, *Physical Review B* 48 (1993) 14884–14891.
- [10] K. Lee, A.J. Heeger, Y. Cao, *Synthetic Metals* 69 (1995) 261–262; K. Lee, A.J. Heeger, *Synthetic Metals* 84 (1997) 715–718.
- [11] P.N. Adams, P.J. Laughlin, A.P. Monkman, *Synthetic Metals* 76 (1996) 157–160; J. Joo, Y.C. Chung, H.G. Song, J.S. Baeck, W.P. Lee, A.J. Epstein, A.G. MacDiarmid, S.K. Jeong, *Synthetic Metals* 84 (1997) 739–740.
- [12] E.R. Holland, S.J. Pomfret, P.N. Adams, A.P. Monkman, *Journal of Physics* 8 (1996) 2991–3002; L. Abell, P.N. Adams, A.P. Monkman, *Polymer* 37 (1996) 5927–5931; L. Abell, S.J. Pomfret, P.N. Adams, A.C. Middleton, A.P. Monkman, *Synthetic Metals* 84 (1997) 803–804.
- [13] P.N. Adams, P. Devasagayam, S.J. Pomfret, L. Abell, A.P. Monkman, *Journal of Physics* 10 (1998) 8293–8303; V. Mottaghitlab, G.M. Spinks, G.G. Wallace, *Polymer* 47 (2006) 4996–5002.
- [14] V. Sitaram, A. Sharma, S.V. Bhat, K. Mizoguchi, R. Menon, *Physical Review B* 72 (2005), pp. 035209/1–035209/7.
- [15] D. Yang, B.R. Mattes, *Synthetic Metals* 158 (2008) 654–660.
- [16] G. Tzamalīs, N.A. Zaidi, C.C. Homes, A.P. Monkman, *Physical Review B* 66 (2002) 085202–085209.
- [17] J.P. Foreman, A.P. Monkman, *Journal of Physical Chemistry A* 107 (2003) 7604–7610.
- [18] A.K. Mukherjee, R. Menon, *Pramana Journal of Physics* 58 (2002) 233–239.
- [19] P.K. Kahol, N.J. Pinto, *Solid State Communications* 124 (2002) 195–197.
- [20] V.I. Krinichnyi, *Russian Chemical Bulletin* 49 (2000) 207–233.
- [21] V.I. Krinichnyi, in: S. Schlick (Ed.), *Advanced ESR Methods in Polymer Research*, Wiley, Hoboken, NJ, 2006, pp. 307–338, and references cited therein, see also web site.
- [22] M. Nechtschein, in: F.T.A. Skotheim, R.L. Elsenbaumer, J.R. Reynolds (Eds.), *Handbook of Conducting Polymers*, Marcel Dekker, New York, 1997, pp. 141–163.
- [23] K. Mizoguchi, S. Kuroda, in: H.S. Nalwa (Ed.), *Handbook of Organic Conductive Molecules and Polymers*, vol. 3, John Wiley & Sons, Chichester, New York, 1997, pp. 251–317.
- [24] N.S. Sariciftci, A.J. Heeger, Y. Cao, *Physical Review B* 49 (1994) 5988–5992.
- [25] N.S. Sariciftci, A.C. Kolbert, Y. Cao, A.J. Heeger, A. Pines, *Synthetic Metals* 69 (1995) 243–244.
- [26] W.P. Lee, A.J. Epstein, K.R. Brennehan, A.D. Gudmundsdottir, M.S. Platz, P.K. Kahol, A.P. Monkman, *Synthetic Metals* 101 (1999) 819–820.
- [27] N.S. Sariciftci (Ed.), *Primary Photoexcitations in Conjugated Polymers: Molecular Exciton versus Semiconductor Band Model*, World Scientific Publ., Singapore, 1997.
- [28] V.I. Krinichnyi, *Synthetic Metals* 108 (2000) 173–222.
- [29] V.I. Krinichnyi, A.L. Konkin, P. Devasagayam, A.P. Monkman, *Synthetic Metals* 119 (2001) 281–282.
- [30] A.L. Konkin, V.G. Shtyrlin, R.R. Garipov, A.V. Aganov, A.V. Zakharov, V.I. Krinichnyi, P.N. Adams, A.P. Monkman, *Physical Review B* 66 (2002), pp. 075203/1–075203/11.
- [31] P.N. Adams, P.J. Laughlin, A.P. Monkman, A.M. Kenwright, *Polymer* 37 (1996) 3411–3417, United Kingdom Pat., 2287030 (1997).
- [32] V.I. Krinichnyi, S.V. Tokarev, H.K. Roth, M. Schrödner, B. Wessling, *Synthetic Metals* 152 (2005) 165–168; V.I. Krinichnyi, H.K. Roth, M. Schrödner, B. Wessling, *Polymer* 47 (2006) 7460–7468; V.I. Krinichnyi, S.V. Tokarev, H.K. Roth, M. Schrödner, B. Wessling, *Synthetic Metals* 156 (2006) 1368–1377.
- [33] F.J. Dyson, *Physical Review B* 98 (1955) 349–359.
- [34] A.C. Chapman, P. Rhodes, E.F.W. Seymour, *Proceedings of the Physical Society B* 70 (1957) 345–360.
- [35] P. Wzietek, F. Creuzet, C. Bourbonnais, D. Jerome, K. Bechgaard, P. Batail, *Journal de Physique I* 3 (1993) 171–201.

- [36] S.V. Vonsovskii, *Magnetism* (Russ.), Nauka, Moscow, 1971; H. Salavagione, G.M. Morales, M.C. Miras, C. Barbero, *Acta Polymerica* 50 (1999) 40–44.
- [37] M. Iida, T. Asaji, M.B. Inoue, M. Inoue, *Synthetic Metals* 55 (1993) 607–612.
- [38] V.I. Krinichnyi, H.K. Roth, G. Hinrichsen, F. Lux, K. Lüders, *Physical Review B* 65 (2002), pp. 155205/1–155205/14.
- [39] J.S. Blakemore, *Solid State Physics*, Cambridge University Press, Cambridge, 1985.
- [40] B. Beau, J.P. Travers, E. Banka, *Synthetic Metals* 101 (1999) 772; B. Beau, J.P. Travers, F. Genoud, P. Rannou, *Synthetic Metals* 101 (1999) 778.
- [41] E. Houze, M. Nechtschein, *Physical Review B* 53 (1996) 14309–14318.
- [42] J.M. Williams, J.R. Ferraro, R.J. Thorn, K.D. Carlson, U. Geiser, H.H. Wang, A.M. Kini, M.H. Whangbo, *Organic Superconductors (Including Fullerenes): Synthesis, Structure, Properties, and Theory*, Prentice-Hall, Inc., Englewood Cliffs, New Jersey, 1992.
- [43] L. Forró, G. Sekretarczyk, M. Krupski, D. Schweitzer, H.J. Keller, *Physical Review B* 35 (1987) 2501–2504.
- [44] V.I. Krinichnyi, *Journal of Physical Chemistry B* 112 (2008) 9746–9752; V.I. Krinichnyi, *Journal of Chemical Physics* 129 (2008) 134510–134518.
- [45] J.M. Ginder, A.J. Epstein, *Physical Review B* 41 (1990) 10674–10685.
- [46] S.E. Barnes, *Advances in Physics* 30 (1981) 801–938; V.A. Atsarkin, V.V. Demidov, *Journal of Experimental and Theoretical Physics* 86 (1998) 572–577.
- [47] V.I. Krinichnyi, S.D. Chemerisov, Y.S. Lebedev, *Physical Review B* 55 (1997) 16233–16244.
- [48] H.A. Kuska, M.T. Rogers, in: E.T. Kaiser, L. Kevan (Eds.), *Radical Ions*, vol. 13, John Wiley & Sons, New York, 1968, p. 31, Chapter 13.
- [49] A.L. Buchachenko, A.M. Vasserman, *Stable Radicals* (Russ.), Khimija, Moscow, 1973.
- [50] S.A. Altshuler, B.M. Kozirev, *Electron Paramagnetic Resonance of Compounds of Elements of Intermediate Groups* (Russ.), Nauka, Moscow, 1972.
- [51] A. Abragam, *The Principles of Nuclear Magnetism*, Clarendon Press, Oxford, 1961.
- [52] N.F. Mott, E.A. Davis, *Electronic Processes in Non-Crystalline Materials*, Clarendon Press, Oxford, 1979.
- [53] I.G. Austin, N.F. Mott, *Advances in Physics* 18 (1969) 41–102.
- [54] L. Pietronero, *Synthetic Metals* 8 (1983) 225–231.
- [55] J. Joo, Z. Oblakowski, G. Du, J.P. Pouget, E.J. Oh, J.M. Weisinger, Y. Min, A.G. MacDiarmid, A.J. Epstein, *Physical Review B* 49 (1994) 2977–2980; Y.Z. Wang, J. Joo, C.H. Hsu, A.J. Epstein, *Synthetic Metals* 68 (1995) 207–211.